Lee Hanna (Orcid ID: 0000-0002-2003-4377)

Muri Helene (Orcid ID: 0000-0003-4738-493X)

Chadburn Sarah (Orcid ID: 0000-0003-1320-315X)

Lawrence David, M (Orcid ID: 0000-0002-2968-3023)

The response of permafrost and high latitude ecosystems under large scale stratospheric aerosol injection and its termination

Hanna Lee[1], Altug Ekici[2,3], Jerry Tjiputra[1], Helene Muri[4], Sarah Chadburn[5], David M. Lawrence[6], Jörg Schwinger[1]

[1]NORCE Norwegian Research Centre, Bjerknes Centre for Climate Research, Bergen, Norway

[2]Climate and Environmental Physics, Physics Institute, University of Bern, Bern, Switzerland

[3]Oeschger Centre for Climate Change Research, University of Bern, Bern, Switzerland

[4]Industrial Ecology Programme, Department of Energy and Process Engineering, Norwegian University of Science and Technology, Trondheim, Norway

[5]University of Exeter, College of Engineering, Mathematics and Physical Sciences, Exeter, UK [6]Climate and Global Dynamics Division, National Centre for Atmospheric Research, Boulder, Colorado, USA

Corresponding author: Hanna Lee (hanna.lee@norceresearch.no)

Key Points:

- Stratospheric aerosol injection may help slow down the current rate of permafrost degradation

- Regional differences in temperature and precipitation, which led to differences in the timing of permafrost degradation up to 40 years.

- It is important to investige the regional effects of climate engineering, particularly in high latitude ecosystems.

Abstract

Climate engineering arises as one of the potential methods that could contribute to meeting the 1.5ºC global warming target agreed under the Paris Agreement. We examine how permafrost and high latitude vegetation respond to large scale implementation of climate engineering. Specifically, we explore the impacts of applying the solar radiation management method of stratospheric aerosol injections (SAI) on permafrost temperature and the global extent of near-surface permafrost area. We compare the RCP8.5 and RCP4.5 scenarios to several SAI deployment scenarios using the Norwegian Earth System Model (CE1: moderate SAI scenario to bring down global mean warming in RCP8.5 to the RCP4.5 level, CE2: aggresive SAI scenario to maintain global mean temperature toward the preindustrial level). We show that large scale application of SAI may help slow down the current rate of permafrost degradation for a wide range of emission scenarios. Between the RCP4.5 and CE1 simulations, the differences in the permafrost degradation may be attributed to spatial variations in surface air temperature, rainfall, snowfall, which lead to differences in the timing of permafrost degradation up to 40 years. Although atmospheric temperatures in CE1

and RCP4.5 simulations are similar, net primary production is higher in CE1 due to CO_2 fertilization. Our investigation of permafrost extent under large-scale SAI application scenarios suggest that circum-Arctic permafrost area and extent is rather sensitive to temperature changes created under such SAI application. Our results highlight the importance of investigating the regional effects of climate engineering, particularly in high latitude ecosystems.

1 Introduction

The Paris Agreement, adopted under the United Nations Framework Convention on Climate Change (UNFCCC), aims at "holding the increase in the global average temperature to well below 2°C above pre-industrial levels and pursuing efforts to limit the temperature increase to 1.5°C above pre-industrial level" (UNFCCC, 2015). In order to meet this agreement, countries have submitted detailed national emission reduction plans starting the year 2020 (UNFCCC, 2015). There is, however, growing scientific evidence that the 1.5°C target cannot be reached unless 1) more ambitious emission reductions are pursued or 2) negative emissions technology are employed (Rogelj et al., 2016; Schleussner et al., 2016).

Climate engineering (CE), broadly defined as deliberate large-scale climate interventions, have been proposed as potential alternative or fallback plans for reducing the radiative impacts of CO_2 emissions (Crutzen, 2006; IPCC, 2013, 2018). Additionally, CE may be used to buy time to reduce emissions while new mitigation methods and technologies are being developed (Wigley, 2006). Solar radiation management (SRM) methods are being investigated for their potential to reduce excess warming from anthropogenic climate change (EuTRACE, 2015; NAS, 2015). The idea of SRM is to alter the radiation budget of the Earth to offset the increased radiative forcing caused by anthropogenic greenhouse gases. Among them, one of the most discussed method is stratospheric aerosol injection (SAI), which

mimics the effect of large volcanic eruptions in nature. The excess sulphur aerosol introduced by SAI or volcanic eruptions induces negative radiative forcing by scattering more incoming solar radiation back to the space, leading to net cooling of surface temperature, which have also been demonstrated to have extended impacts on the land carbon cycle (Robock, 2013; Tjiputra & Otterå, 2011).

Potentially, SAI application would affect both the physical climate and global-scale biogeochemical processes. When changing solar radiation at the surface, temperature and precipitation patterns can cause the land and ocean biosphere carbon sink and source capabilities to change. Recent studies investigating the impacts of SAI on global and regional climate (*e.g.* Berdahl et al., 2014; Kravitz et al., 2015; Muri et al., 2018) suggest that the overall effect of SAI is the amelioration of global scale warming by reducing the incoming shortwave radiation. Therefore, there are large impacts on land and ocean carbon cycling on a global scale (Lauvset et al., 2017; Muri et al., 2018; Tjiputra et al., 2016). Our previous study using SAI method showed that global mean surface temperature can be reduced by 2ºC by the year 2100 and 5ºC by the year 2200 compared to its baseline RCP8.5 scenario (Tjiputra et al., 2016). However, analyses in different regions exhibit contrasting responses from the global mean and thus there is still a need to investigate the regional impacts of SAI application.

Permafrost, defined as ground material frozen for two or more consecutive years, is a very important component of high latitude ecosystems. Models suggest a present day degradation rate of almost 1 million km^2 per decade (*e.g.* Lawrence et al., 2012) and it is expected to continue degrading with the warming climate (Koven et al., 2013; Slater & Lawrence, 2013). Modeling studies emphasize that permafrost can play a major role in carbon-climate feedbacks via permafrost carbon release (Schuur et al., 2015). Yet, estimating the timing and magnitude of permafrost carbon release is challenging, in part due to differing projections of future permafrost extent in different models (McGuire et al., 2018; Schuur et

al., 2015; Slater & Lawrence, 2013). Therefore, the fate of permafrost under different emission scenarios contributes to the large uncertainty in projections of climate and its feedback cycles (MacDougall et al., 2015). This adds to the difficulty of pinning down the remaining carbon budget for limiting warming to 1.5°C. In addition, the response of permafrost, possible carbon release, and its feedback to climate under long term CE application has so far not been exclusively investigated.

In this study, we address how permafrost and high latitude vegetation responds to large-scale implementation of CE. Specifically, we explore the impacts of applying SAI on permafrost temperature and the global extent of near-surface permafrost area under different scenarios. In addition to SRM application, we investigate the impacts of abrupt large-scale SRM termination. We performed a set of idealized simulations following the RCP8.5 scenario but with application of SAI starting in year 2020 to (1) achieve a similar level of surface temperature as in the RCP4.5 scenario and (2) stabilize surface temperatures at 2020 levels until the year 2200. In a third simulation, the strong SAI application of simulation (2) was terminated in year 2100.

We conducted these simulations using an Earth System Model, NorESM1-ME (see Section 2.1), to understand the physical responses of permafrost soil to SRM. Our results provide valuable insights into the response of permafrost under climate engineering. To our knowledge, this study is the first to explicitly estimate the response of permafrost under SRM application.

2 Methods

2.1 Model description (NorESM)

We use the fully coupled Norwegian Earth system model (NorESM1-ME) to simulate the impact of idealized SAI scenarios under a high-CO_2 RCP8.5 future scenario. NorESM1-ME is based on the Community Earth System Model version 1 (CESM1; Gent et al., 2011). The main differences between the NorESM1-ME and CESM1 are: (1) an improved atmospheric chemistry-aerosol-cloud module (Kirkevag et al., 2013), (2) the ocean circulation model, which is based on the Miami Isopycnic Coordinate Ocean Model (MICOM) with extensive modifications (Bentsen et al., 2013), and (3) the ocean biogeochemical model, which originated from the Hamburg Oceanic Carbon Cycle (HAMOCC) model (Tjiputra et al., 2013). Both the land and atmospheric components have approximately 2-degree horizontal resolution, whereas the ocean model is configured with 1-degree horizontal resolution and with 53 isopycnal layers.

2.2 Permafrost representation

The land component of NorESM1-ME is CLM4 (Lawrence et al., 2011), which has been employed and developed in permafrost applications for almost a decade. CLM4 includes permafrost processes that allow simulation of key thermal and hydrological processes and is considered one of the most advanced land surface schemes with respect to permafrost (Lawrence & Slater, 2008; Lawrence et al., 2008; Slater & Lawrence, 2013). The permafrost distribution in CLM4 simulations matches the observed distribution reasonably well, with the southern edge of permafrost accurately captured across Siberia, Alaska, and Canada (Lawrence et al., 2012). Near-surface permafrost extent in CLM4 is on the high end of the observed estimates: 14.2 million km^2 (Lawrence et al., 2012). This is comparable to the current day estimation of 16.2 million km^2 (Brown et al., 2002).

Our Earth system model, as is the case with all CMIP5 (Coupled-climate Model Intercomparison Projects 5) models, does not have the capacity to estimate the permafrost carbon-climate feedback. There are several known limitations in representing soil carbon in CLM4 simulations, particularly in permafrost soils. The key limitations include 1) processes that govern the accumulation of soil organic material in the cold, moist high-latitude climate regime such as decomposition constraints due to anoxia and the mixing of organic matter into the soil through cryoturbation (Koven et al., 2009), 2) lack of vertically-resolved carbon in soils (Koven et al., 2017; Koven et al., 2013), and 3) higher climatological temperature sensitivity of soil carbon in colder climates (Koven et al., 2017). The model does not explicitly take into account permafrost carbon release into the global carbon cycling. For this reason, we do not analyze the permafrost carbon-climate feedback, but focus on vegetation carbon fluxes in our study. Additionally, we note that although CLM4 does prognostically calculate soil carbon content, soil carbon content is not used to set the thermal and hydrological soil properties.

2.3 Experimental design

As a baseline, we used the historical (1850-2005), and RCP8.5 future scenario (2006-2100) according to the CMIP5 experimental protocol (Taylor et al., 2012). In addition, a RCP4.5 future scenario simulation (2006-2100) was performed for comparison. RCP8.5 was extended to 2200 as described in Tjiputra et al., (2016). Prior to these simulations, NorESM1-ME was spun up fully coupled for more than 1000 model years at preindustrial boundary conditions. For the last 100 years of the pre-industrial period, the model had reached a quasi-equilibrium state with the global mean atmospheric CO_2 concentration fluctuating between 282 and 286 ppm.

For the SAI experiments (Table 1), we implemented a linear increase in stratospheric mass mixing ratio of SO_4, scaled to the observed monthly spatial distribution of SO_4 in the year following the 1991 Mount Pinatubo eruption (*i.e.* September 1991 to August 1992) according to (Ammann et al., 2003). As the Pinatubo eruption occurred in the tropics, maximum aerosol forcing is located in the low latitudes and declines towards the poles throughout the experiment period. NorESM1-ME does not take into account sulfate interactions with stratospheric ozone. A thorough description of the idealized forcing including its spatial and temporal evolutions are illustrated in Tjiputra et al., (2016).

Two CE forcings (CE1 and CE2) were implemented to represent idealized SAI-based climate engineering for the 2020-2100 period. CE1 represents a linear increase of stratospheric aerosol from the reference level (at 2020) to 2x Pinatubo levels (at 2100), whereas CE2 reaches 5x Pinatubo by 2100. The CE1 forcing was targeted to bring the projected global mean surface temperature under the RCP8.5 scenario down to a level similar to that in the RCP4.5 scenario by the end of the 21st century. The stronger CE2 forcing was developed to assess the impact of an aggressive future SAI application scenario. The CE2 forcing scenario continues to 2200 while maintaining 5x Pinatubo forcing in the 22nd century. The CE1 and CE2 scenarios were designed for a high signal-to-noise ratio to assess the nature of the response. Due to the model limitations, our idaelized SAI scenario neglect the evolution of aerosol particle size in the stratosphere (i.e., higher concentrations would lead to particle coagulation and larger sizes, which reduce their efficiency in scattering incoming short-wave radiation (Niemeier et al., 2011). Lastly, an additional simulation, branched from CE2, was performed to examine the effects of SAI termination at 2100, over the following century (CE2T).

In all simulations, we applied a fully interactive carbon cycle configuration, which prescribes anthropogenic CO_2 emissions and prognostically simulates regionally varying atmospheric CO_2 concentration. Under RCP4.5, fossil fuel emissions peak at roughly 11 Pg C yr^{-1} around the 2040s and decline towards 2100. Under RCP8.5, emissions increase to 28.5 Pg C yr^{-1} by the end of the 21st century. For the extended (2101-2200) RCP8.5 simulations, we applied constant forcings, *i.e.*, prescribed land use change, ozone concentration, aerosol deposition, and atmospheric greenhouse gas boundary conditions taken from the year 2100. The CO_2 emissions, however, remain at 2100 emission level after 2100, before linearly declining from 2150 onwards according to Meinshausen et al., (2011).

3 Results and Discussion

3.1 Deep soil temperature and near-surface permafrost extent

High latitude (described in our study as 55-85°N) absorbed solar radiation at the surface under SAI application exhibited expected results (Figure 1A); CE1 follows similar radiation levels to the RCP4.5 scenario, CE2 maintains stable radiation levels similar to the beginning of the SAI application, and CE2T rapidly increases to the level of the RCP8.5 scenario after termination of SAI in year 2100. As a result, high latitude surface air temperature (hereafter TSA, air temperature at 2 m, averaged over land regions 55°N to 85°N) in CE1 and CE2 is significantly lower compared to the Control RCP8.5 scenario. Under CE1, mean high latitude TSA is maintained close to its target level (RCP4.5). There is a noticeable difference in TSA between CE1 and RCP4.5 in the high latitudes by the end of the 21st century, which is much larger than the the global mean difference between these two scenarios (Tjiputra et al., 2016). Although the CE1 experiment is designed to target global TSA of the RCP4.5 scenario, shortwave-based aerosol geoengineering methods tend to exhibit higher Arctic mean annual temperature (1-2°C; Muri et al., 2018).

Under CE2, TSA remains stable at 2020 levels and hence substantially lower than the control RCP8.5 scenario until the year 2100, and slowly increases approximately by 4°C thereafter (Figure 1B). This is due to the experimental design, where the CE2 forcing remains constant after the year 2100, while atmospheric CO_2 concentration continues to increase. After termination of SAI application in CE2T, TSA exhibits a rapid increase, coming close to the level of the RCP8.5 scenario within 10 years, but remaining around 1-2°C lower. Rapid warming after termination of SAI was exhibited in most models in GeoMIP (Geoengineering Model Intercomparison Project) study (Jones et al., 2013), and the majority of the model experiments also do not reach the same level of TSA as the RCP8.5 scenario, likely due to reduced ocean heat uptake during the CE (Hong et al., 2017; Muri et al., 2018). Mean high latitude soil temperatures exhibit a similar pattern to TSA, with a slightly lower rate of change (Figure 1C).   Total near-surface permafrost area, defined here as the integrated area of grid boxes between 25-85°N that contain at least one soil layer within the top 3.8 m that remains below 0°C throughout the year, for 2 or more consecutive years, rapidly decreases under the RCP8.5 scenario, from 11.5 million km^2 in 2020 to ~3 million km^2 in the year 2100 (Figure 1D). This estimate is in line with previous model simulations using the RCP8.5 projection periods (Lawrence et al., 2012). As expected, near-surface permafrost area declines more slowly under the lower emissions scenario RCP4.5 and under the CE1 simulation, compared to the RCP8.5 scenario. The CE2 application maintains near-surface permafrost area at a level similar to the year 2020 until 2100. Interestingly, near-surface permafrost area increases slightly towards the end of the 21st century in CE2, where radiation level drops below the level of year 2020.

Soil temperature at 3.0 m depth responds rather quickly to the termination of large-scale SAI application. As a result, estimated permafrost area exhibits a sharp decline upon SAI termination from the year 2100, and reaches a similar level to the RCP8.5 scenario after

approximately 20 years. There is approximately 1 million km^2 difference in the total permafrost area between CE2T and the RCP8.5 scenario after 20 years from SAI termination. However, by the year 2200 the total permafrost area is similar under both scenarios, where permafrost area is confined to only the northernmost part of the Arctic.

Mean TSA and soil temperature show similar patterns in CE1 and RCP4.5 scenarios until the year 2070, but CE1 becomes warmer than the RCP4.5 scenario when the radiative forcing in the RCP4.5 scenario stabilizes, starting around 2070. This is due to the differnce in the forcing scenarios between RCP4.5 and baseline RCP8.5 scenario, where RCP4.5 scenario has stronger mitigation efforts portrayed in its forcing data whereas RCP8.5 does not. As a result, total permafrost area in the two simulations differs by approximately 1.5 million km^2 at the end of the 21st century (Figure 1D).

A closer look at regional differences in the RCP4.5 and CE1 simulations suggest that the differences in the permafrost degradation (Figure 2) may be attributed to spatial variations between TSA, rainfall, snowfall, which lead to small differences in soil temperature and soil moisture in the RCP4.5 scenario and CE1 (Figure 3). These areas include eastern Siberia, where the CE1 simulation is warmer than RCP4.5 and the majority of difference in permafrost extent is from this region at the end of the 21st century. In addition, there is higher amount of snowfall in this area, which can play an insolating effect. There is a regional variation in the magnitude of change in TSA and precipitation following SAI application, where the high latitude TSA tends to be warmer although the general response in TSA is similar overall on a global scale (Ricke et al., 2010). Some of the grid points that show permafrost degradation only under CE1 exhibit similar overall patterns in TSA between the RCP4.5 and CE1 scenarios (Supplementary Figure 1 & 2), where TSA in CE1 remains similar to the RCP4.5 scenario and CE1 becomes warmer around the year 2070. Soil temperature at 3.0 m can be more distinctively different between the two scenarios. This

results in a difference of over 40 years' in the timing of permafrost degradation in some grid cells (see panel Supplementary Figure 1f & 2f).

The regional variations are in part due to the nature of forcing scenarios, where the aerosol forcings and land cover change are different between the RCP4.5 and RCP8.5 scenarios (Thomson et al., 2011). Increased forest cover in the southern edge of the permafrost area towards the end of the century in the RCP4.5 scenario compared to RCP8.5 may have played a role in the regional variation between CE1 and RCP4.5 simulations as changes in surface albedo and snow cover associated with land cover change may influence regional variations. In this case, however, land cover change may not be very important in high latitude ecosystems.

3.2 High latitude vegetation carbon responses under SAI application

Net primary production (NPP) in high latitude ecosystems is lower under CE2 application than the reference RCP8.5 scenario (Figure 4A). Compared to previous studies, where global NPP is less sensitive to SAI application due to large masking from the tropics (Jones et al., 2013; Muri et al., 2018), our analysis emphasizes that high latitude vegetation response is sensitive to SAI application, likely because this particular ecosystem is temperature limited (Keenan & Riley, 2018). Although atmospheric temperatures in CE1 and RCP4.5 simulations are similar, NPP is higher in CE1. This is likely due to higher atmospheric CO_2 concentrations, as vegetation is responding to CO_2 fertilization. We note that CLM4 includes a representation of N limitation, and hence the response of vegetation to CO_2 fertilization in NorESM is more plausible in terms of N availability compared to other CMIP5 models (Zaehle et al., 2015). The change in the ratio of direct to diffuse radiation under SAI application will also be beneficial for NPP (Xia et al., 2016), as diffuse light can penetrate through the canopy to the shaded leaves. The NPP increases rapidly in CE2T when SAI is terminated, catching up to the same level of NPP as the Control RCP8.5 scenario. This

suggests that high latitude NPP is much limited by the lower surface temperatures under strong SAI application in our model simulations.

Carbon use efficiency, estimated by the ratio of NPP/GPP (Gross Primary Production), describes the control on carbon storage in ecosystems and is an important measure for understanding the source-sink dynamics of an ecosystem (Allison et al., 2010). Our results show that high latitude carbon use efficiency is more sensitive to changes in temperature than to atmospheric CO_2 concentrations (Figure 4B). This is in line with general understanding that carbon use efficiency decreases with higher temperature, and illustrates that the model slightly loses the efficiency of carbon storage in a warmer world (Zhang et al., 2014). Although Glienke et al., (2015) report that the CLM models used in their GeoMIP multi-model analysis exhibit an even distribution of carbon use efficiency across all latitudes around 0.35-0.4, our results illustrate that there is much larger change in carbon use efficiency in high latitude ecosystems under the scenarios we investigated. However, the slight difference in carbon use efficiency shown between CE1 and the RCP4.5 scenario suggests that given similar temperature level, the level of CO_2 concentrations in the atmosphere and surface radiation also affect carbon use efficiency.

4 Summary and Implications

The overall assessment of SAI application simulations in permafrost regions in our study suggest that SAI application may help slow down the current rate of degradation of permafrost under the range of emission scenarios used in our study. Closer investigation of permafrost extent during the SAI application indicates the potential reversibility of permafrost thaw when temperature increase was slowed down or reversed. From these results, we speculate similar effects under low and negative emission scenarios. However, the release of permafrost carbon could still have a large impact on feedbacks to climate and

related tipping points, and is likely irreversible (Boucher et al., 2012).

Our investigation of permafrost extent under large-scale SAI application scenarios illustrates that circum-Arctic permafrost area and extent is rather sensitive to temperature changes created under such SAI application. Permafrost areas experience rapid degradation towards the Control RCP8.5 scenario within 20 years after termination. The speed of permafrost degradation upon SAI termination is approximately 4 times faster than the maximum degradation rate found during the 21st century in RCP8.5. This rate, however, is highly dependent on the choice of scenario and recent studies point out that termination shock should be much less likely, and therefore much less of a risk, than has previously been assumed (Parker & Irvine, 2018). Although, the difference in permafrost extent and temperature even after several decades of SAI termination can lead to some differences in permafrost degradation and permafrost carbon release.

The permafrost carbon feedback is a process that has longer-term implications. In the scenarios where permafrost thaws over the 21st century (RCP8.5, 4.5, and CE1), we may see substantial carbon release over this century, and certainly beyond (as in *e.g.* McGuire et al., 2018). This would lead to additional climate warming in addition to what is simulated here. Our results suggest that the permafrost response to RCP 4.5 and CE1 are similar within the 21st century suggesting that CE would effectively offset this important cabon-cycle feedback, which some estimates have as approximately 27-122 Pg C of reduced emissions in 21st century (Keith et al., 2017). The carbon dioxide release from permafrost thaw has a greater impact on global temperature when atmospheric CO_2 is lower due to the logarithmic dependence of radiative forcing on CO_2 concentrations (*e.g.* Etminan et al., 2016), thus the additional warming would likely be greater in RCP4.5 than in CE1. On the other hand, additional uptake of carbon by vegetation (particularly in warm and high-CO_2 scenarios, Figure 4A) may offset some of the permafrost carbon release.

It is possible that the cumulative permafrost carbon release under RCP8.5 and CE2T may ultimately be different, despite finishing at a similar global temperature and atmospheric CO_2 level, since the total carbon release can depend on the pathway (Gasser et al., 2018). We did not further investigate the effects of permafrost carbon and its potential feedbacks in this study because of known limitations in CLM4. Our study, however, illustrate the importance of investigating the regional effects of SAI application particularly in the high latitude ecosystems. We encourage future investigation towards permafrost carbon climate feedbacks under the large scale application of SAI using more advanced modeling tools, where recent model developments such as a prognostic methane module, vertically-resolved soil carbon, and higher resolution soil layers can help resolve some of the limitations shown in our study. In addition, further modeling efforts to investigate different methods in SAI application to effectively cool high latitudes would be necessary.

Our study strongly suggests that there is a need for more investigation of large scale SAI application in various aspects, particularly different regional impacts and the impacts of SAI termination, for SAI application to be considered as an alternative method of mitigation or a method to buy time until a technological solution arises.

References

Allison, S. D., Wallenstein, M. D., & Bradford, M. A. (2010). Soil-carbon response to warming dependent on microbial physiology. *Nature Geoscience*, *3*(5), 336–340. https://doi.org/10.1038/NGEO846.

Ammann, C., Meehl, G., Washington, W., & Zender, C. (2003). A monthly and latitudinally varying volcanic forcing dataset in simulations of 20th century climate. *Geophysical Research Letters*, *30*(12). https://doi.org/10.1029/2003GL016875.

Bentsen, M., Bethke, I., Debernard, J. B., Iversen, T., Kirkevag, A., Seland, O., et al. (2013). The Norwegian Earth System Model, NorESM1-M - Part 1: Description and basic evaluation of the physical climate. *Geoscientific Model Development*, *6*(3), 687–720. https://doi.org/10.5194/gmd-6-687-2013.

Berdahl, M., Robock, A., Ji, D., Moore, J. C., Jones, A., Kravitz, B., & Watanabe, S. (2014). Arctic cryosphere response in the Geoengineering Model Intercomparison Project G3 and G4 scenarios. *Journal of Geophysical Research-Atmospheres*, *119*(3), 1308–1321. https://doi.org/10.1002/2013JD020627.

Boucher, O., Halloran, P. R., Burke, E. J., Doutriaux-Boucher, M., Jones, C. D., Lowe, J., et al. (2012). Reversibility in an Earth System model in response to CO_2 concentration changes. *Environmental Research Letters*, *7*(2). https://doi.org/10.1088/1748-9326/7/2/024013.

Brown, J., Ferrians Jr., O., Heginbottom, J. A., & Melnikov, E. S. (2002). Circum-Arctic map of permafrost and ground-ice conditions, version 2. National Snow and Ice Data Center, Boulder, CO. Retrieved from http://nsidc.org/data/ggd318.html.

Crutzen, P. J. (2006). Albedo enhancement by stratospheric sulfur injections: A contribution to resolve a policy dilemma? *Climatic Change*, *77*(3–4), 211–219. https://doi.org/10.1007/s10584-006-9101-y.

Etminan, M., Myhre, G., Highwood, E. J., & Shine, K. P. (2016). Radiative forcing of carbon dioxide, methane, and nitrous oxide: A significant revision of the methane radiative forcing. *Geophysical Research Letters*, *43*(24), 12614–12623. https://doi.org/10.1002/2016GL071930.

EuTRACE. (2015). *The European Transdisciplinary Assessment of Climat Engineering: Removing Greenhouse Gases from the Atmosphere and Reflecting Sunlight away from Earth*. Retrieved from http://www.eutrace.org/

Gasser, T., Kechiar, M., Ciais, P., Burke, E. J., Kleinen, T., Zhu, D., et al. (2018). Path-dependent reductions in CO_2 emission budgets caused by permafrost carbon release. *Nature Geoscience*. https://doi.org/10.1038/s41561-018-0227-0.

Gent, P. R., Danabasoglu, G., Donner, L. J., Holland, M. M., Hunke, E. C., Jayne, S. R., et al. (2011). The Community Climate System Model Version 4. *Journal of Climate*, *24*(19), 4973–4991. https://doi.org/10.1175/2011JCLI4083.1.

Glienke, S., Irvine, P. J., & Lawrence, M. G. (2015). The impact of geoengineering on vegetation in experiment G1 of the GeoMIP. *Journal of Geophysical Research-Atmospheres*, *120*(19), 10196–10213. https://doi.org/10.1002/2015JD024202.

Hong, Y., Moore, J. C., Jevrejeva, S., Ji, D., Phipps, S. J., Lenton, A., et al. (2017). Impact of the GeoMIP G1 sunshade geoengineering experiment on the Atlantic meridional overturning circulation. *Environmental Research Letters*, *12*(3), 034009. https://doi.org/10.1088/1748-

9326/aa5fb8.

IPCC. (2013). *Climate Change: The Physical Science Basis. Contribution of Working Group I to the Fifth Assessment Report of the Intergovernmental Panel on Climate Change, edited by: Stocker, T. F., Qin, D., Plattner, G.-K., Tignor, M., Allen, S. K., Boschung, J., Nauels, A., Xia, Y., Bex, V., and Midgley, P. M.* Cambridge, UK and New York, NY, USA,: Cambridge University Press.

IPCC. (2018). *Global warming of 1.5°C. An IPCC Special Report on the impacts of global warming of 1.5°C above pre-industrial levels and related global greenhouse gas emission pathways, in the context of strengthening the global response to the threat of climate change, sustainable development, and efforts to eradicate poverty, V. Masson-Delmotte V., Zhai P., Pörtner H.O., Roberts D., Skea J., Shukla P.R., Pirani A., Moufouma-Okia W., Péan C., Pidcock R., Connors S., Matthews J.B.R., Chen Y., Zhou X., Gomis M.I., Lonnoy E., Maycock M., Tignor M., Waterfield T. (eds.)*

Jones, A., Haywood, J. M., Alterskjaer, K., Boucher, O., Cole, J. N. S., Curry, C. L., et al. (2013). The impact of abrupt suspension of solar radiation management (termination effect) in experiment G2 of the Geoengineering Model Intercomparison Project (GeoMIP). *Journal of Geophysical Research-Atmospheres*, *118*(17), 9743–9752. https://doi.org/10.1002/jgrd.50762.

Keenan, T. F., & Riley, W. J. (2018). Greening of the land surface in the world's cold regions consistent with recent warming. *Nature Climate Change*, *8*(9), 825–828. https://doi.org/10.1038/s41558-018-0258-y.

Kirkevag, A., Iversen, T., Seland, O., Hoose, C., Kristjansson, J. E., Struthers, H., et al. (2013). Aerosol-climate interactions in the Norwegian Earth System Model-NorESM1-M. *Geoscientific Model Development*, *6*(1), 207–244. https://doi.org/10.5194/gmd-6-207-2013.

Koven, C. D., Hugelius, G., Lawrence, D. M., & Wieder, W. R. (2017). Higher climatological temperature sensitivity of soil carbon in cold than warm climates. *Nature Climate Change*, *7*(11), 817–822. https://doi.org/10.1038/NCLIMATE3421.

Koven, C. D., Riley, W. J., & Stern, A. (2013). Analysis of permafrost thermal dynamics and response to climate change in the CMIP5 Earth System Models. *Journal of Climate*, *26*(6), 1877–1900. https://doi.org/10.1175/JCLI-D-12-00228.1.

Koven, C., Friedlingstein, P., Ciais, P., Khvorostyanov, D., Krinner, G., & Tarnocai, C. (2009). On the formation of high-latitude soil carbon stocks: Effects of cryoturbation and insulation by organic matter in a land surface model. *Geophysical Research Letters*, *36*. https://doi.org/10.1029/2009GL040150.

Kravitz, B., Robock, A., Tilmes, S., Boucher, O., English, J. M., Irvine, P. J., et al. (2015). The Geoengineering Model Intercomparison Project Phase 6 (GeoMIP6): simulation design and preliminary results. *Geoscientific Model Development*, *8*(10), 3379–3392. https://doi.org/10.5194/gmd-8-3379-2015.

Keith, D., Wagner, G., Zabel, C.L. (2017). Solar geoengineering reduces atmospheric carbon burden. *Nature Climate Change*, *7(9)*, 617-619. https://doi.org/10.1038/nclimate3376

Lauvset, S. K., Tjiputra, J., & Muri, H. (2017). Climate engineering and the ocean: effects on biogeochemistry and primary production. *Biogeosciences*, *14*(24), 5675–5691. https://doi.org/10.5194/bg-14-5675-2017.

Lawrence, D. M., Oleson, K. W., Flanner, M. G., Thornton, P. E., Swenson, S. C., Lawrence,

P. J., et al. (2011). Parameterization improvements and functional and structural advances in version 4 of the Community Land Model. *Journal of Advances in Modeling Earth Systems*, *3*. https://doi.org/10.1029/2011MS000045.

Lawrence, D. M., & Slater, A. G. (2008). Incorporating organic soil into a global climate model. *Climate Dynamics*, *30*(2–3), 145–160. https://doi.org/10.1007/s00382-007-0278-1.

Lawrence, D. M., Slater, A. G., & Swenson, S. C. (2012). Simulation of present-day and future permafrost and seasonally frozen ground conditions in CCSM4. *Journal of Climate*, *25*(7), 2207–2225. https://doi.org/10.1175/JCLI-D-11-00334.1.

Lawrence, D. M., Slater, A. G., Romanovsky, V., & Nicolsky, D. (2008). Sensitivity of a model projection of near-surface permafrost degradation to soil column depth and representation of soil organic matter. *Journal of Geophysical Research-Earth Surface*, (113), F02011, doi:10.1029/2007JF000883.

MacDougall, A. H., Zickfeld, K., Knutti, R., & Matthews, H. D. (2015). Sensitivity of carbon budgets to permafrost carbon feedbacks and non-CO2 forcings. *Environmental Research Letters*, *10*(12). https://doi.org/10.1088/1748-9326/10/12/125003.

McGuire, A. D., Lawrence, D. M., Koven, C., Clein, J. S., Burke, E., Chen, G., et al. (2018). Dependence of the evolution of carbon dynamics in the northern permafrost region on the trajectory of climate change. *Proceedings of the National Academy of Sciences of the United States of America*, *115*(15), 3882–3887. https://doi.org/10.1073/pnas.1719903115.

Meinshausen, M., Smith, S. J., Calvin, K., Daniel, J. S., Kainuma, M. L. T., Lamarque, J.-F., et al. (2011). The RCP greenhouse gas concentrations and their extensions from 1765 to 2300. *Climatic Change*, *109*(1–2, SI), 213–241. https://doi.org/10.1007/s10584-011-0156-z.

Muri, H., Tjiputra, J., Otterå, O. H., Adakudlu, M., Lauvset, S. K., Grini, A., et al. (2018). Climate response to aerosol geoengineering: A multimethod comparison. *Journal of Climate*, *31*(16), 6319–6340. https://doi.org/10.1175/JCLI-D-17-0620.1.

NAS. (2015). *Climate Intervention: Reflecting Sunlight to Cool Earth*. Washington, DC, USA: The National Academies Press.

Niemeier, U., Schmidt, H., & Timmreck, C. (2011), The dependency of geoengineered sulfate aerosol on the emission strategy, *Atmospheric Science Letters*, *12*, 189–194, doi:10.1002/asl.304.

Parker, A., & Irvine, P. J. (2018). The Risk of Termination Shock From Solar Geoengineering, *Earth's Future, 9999*. https://doi.org/10.1002/2017EF000735.

Ricke, K. L., Morgan, G., & Allen, M. R. (2010). Regional climate response to solar-radiation management. *Nature Geoscience*, *3*(8), 537–541. https://doi.org/10.1038/ngeo915.

Robock, A. (2013). The latest on volcanic eruptions and climate. *Eos Trans. AGU*, *94*(35), 305.

Rogelj, J., den Elzen, M., Hoehne, N., Fransen, T., Fekete, H., Winkler, H., et al. (2016). Paris Agreement climate proposals need a boost to keep warming well below 2 degrees C. *Nature*, *534*(7609), 631–639. https://doi.org/10.1038/nature18307.

Schleussner, C.-F., Rogelj, J., Schaeffer, M., Lissner, T., Licker, R., Fischer, E. M., et al. (2016). Science and policy characteristics of the Paris Agreement temperature goal. *Nature Climate Change*, *6*(9), 827–835. https://doi.org/10.1038/NCLIMATE3096.

Schuur, E. A. G., McGuire, A. D., Schaedel, C., Grosse, G., Harden, J. W., Hayes, D. J., et al. (2015). Climate change and the permafrost carbon feedback. *Nature*, *520*(7546), 171–179. https://doi.org/10.1038/nature14338.

Slater, A. G., & Lawrence, D. M. (2013). Diagnosing present and future permafrost from climate models. *Journal of Climate*, *26*(15), 5608–5623. https://doi.org/10.1175/JCLI-D-12-00341.1.

Taylor, K. E., Stouffer, R. J., & Meehl, G. A. (2012). An overview of CMIP5 and the experiment design. *Bulletin of the American Meteorological Society*, *93*(4), 485–498. https://doi.org/10.1175/BAMS-D-11-00094.1.

Thomson, A. M., Calvin, K. V., Smith, S. J., Kyle, G. P., Volke, A., Patel, P., et al. (2011). RCP4.5: a pathway for stabilization of radiative forcing by 2100. *Climatic Change*, *109*(1–2), 77–94. https://doi.org/10.1007/s10584-011-0151-4.

Tjiputra, J. F., Grini, A., & Lee, H. (2016). Impact of idealized future stratospheric aerosol injection on the large-scale ocean and land carbon cycles. *Journal of Geophysical Research-Biogeosciences*, *121*(1), 2–27. https://doi.org/10.1002/2015JG003045.

Tjiputra, J. F., & Otterå, O. H. (2011). Role of volcanic forcing on future global carbon cycle, *Earth System Dynamics*, 2, 53–67, https://doi.org/10.5194/esd-2-53-2011.

Tjiputra, J. F., Roelandt, C., Bentsen, M., Lawrence, D. M., Lorentzen, T., Schwinger, J., et al. (2013). Evaluation of the carbon cycle components in the Norwegian Earth System Model (NorESM). *Geoscientific Model Development*, *6*(2), 301–325. https://doi.org/10.5194/gmd-6-301-2013.

UNFCCC. (2015). *Adoption of the Paris Agreement United Nations Framework Convention on Climate Change*. Geneva: United Nations Office.

Wigley, T. M. L. (2006). A combined mitigation/geoengineering approach to climate stabilization. *Science*, *314*(5798), 452–454. https://doi.org/10.1126/science.1131728.

Xia, L., Robock, A., Tilmes, S., & Neely, R. R. (2016). Stratospheric sulfate geoengineering could enhance the terrestrial photosynthesis rate. *Atmospheric Chemistry and Physics*, *16*(3), 1479–1489. https://doi.org/10.5194/acp-16-1479-2016.

Zaehle, S., Jones, C. D., Houlton, B., Lamarque, J.-F., & Robertson, E. (2015). Nitrogen Availability Reduces CMIP5 Projections of Twenty-First-Century Land Carbon Uptake. *Journal of Climate*, *28*(6), 2494–2511. https://doi.org/10.1175/JCLI-D-13-00776.1.

Zhang, Y., Yu, G., Yang, J., Wimberly, M. C., Zhang, X., Tao, J., et al. (2014). Climate-driven global changes in carbon use efficiency. *Global Ecology and Biogeography*, *23*(2), 144–155. https://doi.org/10.1111/geb.12086.

Tables

Table 1. The summary of performed model simulations

Simulation	Description	Period	Stratospheric Aerosol Injection forcing
RCP4.5	RCP4.5	2020-2100	None
RCP8.5	RCP8.5	2020-2200	None
CE1	RCP8.5 + CE1	2020-2100	Linearized up to 2x Pinatubo (2020-2100)
CE2	RCP8.5 + CE2	2020-2200	Linearized up to 5x Pinatubo (2020-2100) and remained constant at 5x Pinatubo (2101-2200)
CE2T	CE2 termination	2101-2200	Branched out from CE2 with termination of CE
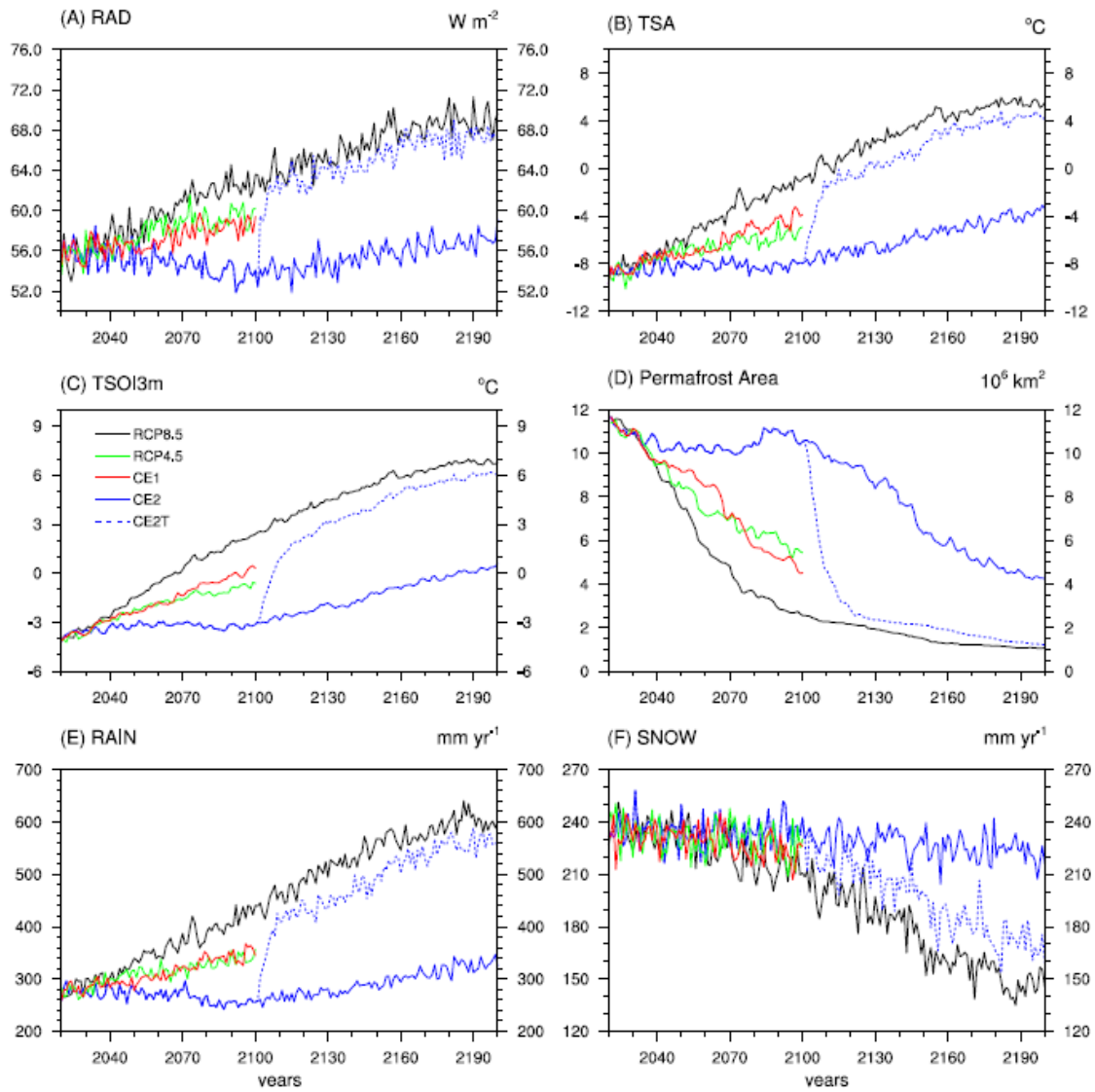
Figure 1. Key high latitude (55-85°N) land biogeophysics parameters for RCP4.5, RCP8.5, CE1, CE2, and CE2T simulations (A) RAD: absorbed solar radiation, (B) TSA: atmospheric temperature at 2 m, (C) TSOI3m: soil temperature at 3 m, (D) Permafrost Area: total area of permafrost, (E) RAIN: mean annual rainfall, and (F) SNOW: mean annual snowfall. The values are mean of 55-85°N except (D), which indicates the total near surface permafrost area at 25-85°N.
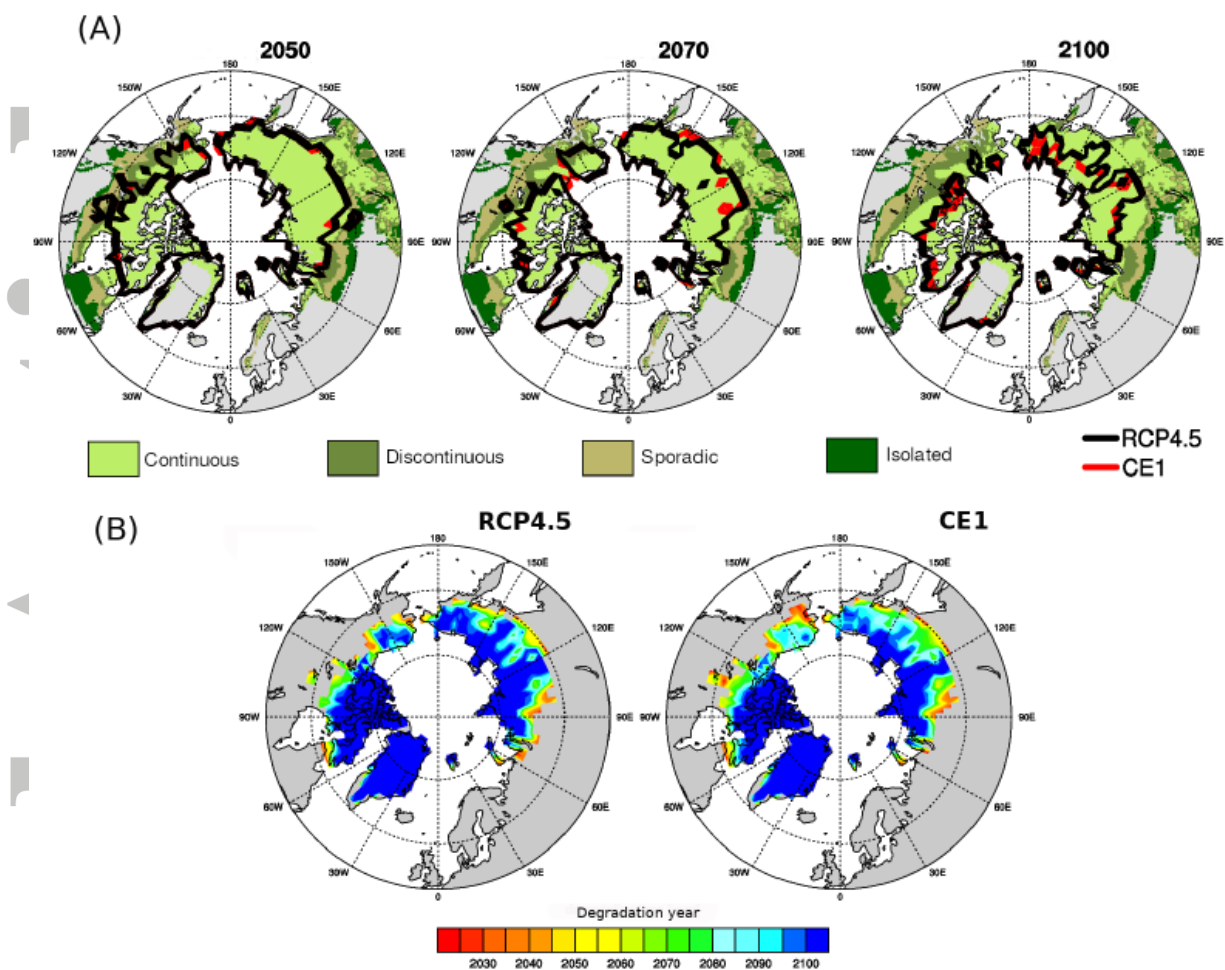
Figure 2

Figure 2. (A) Circum-Arctic map of permafrost extent comparing the RCP4.5 scenario (black) and CE1 simulations (red). Different colors indicate Northern Hemisphere permafrost extent according to the International Permafrost Association's permafrost map (Brown et al., 2002) in the order of continuous, discontinuous, sporadic, and isolated. (B) Circum-Arctic map of permafrost extent and the year of permafrost degradation.
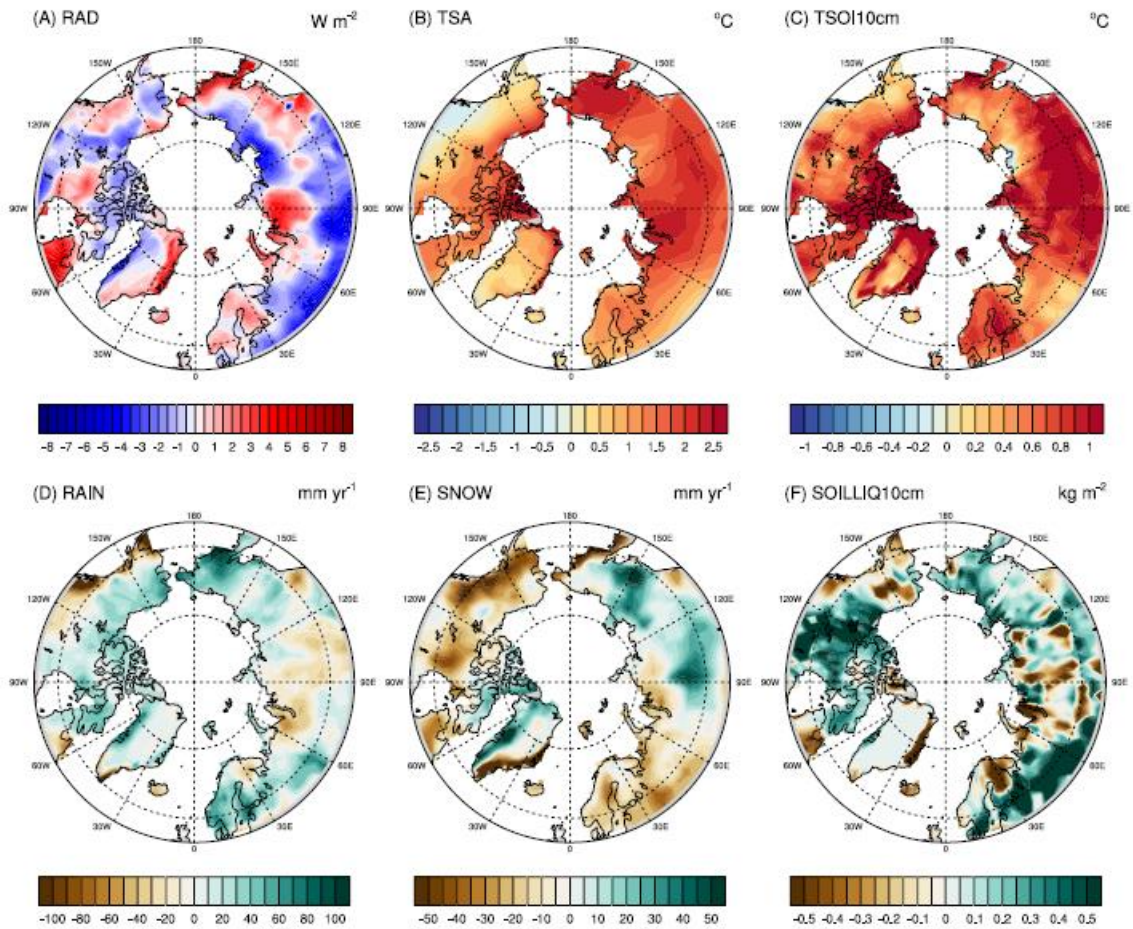
Figure 3. The difference between RCP4.5 and CE1 scenarios (CE1 – RCP4.5) in decadal

mean (2091 to 2100) (A) RAD: absorbed solar radiation, (B) TSA: air temperature at 2 m,

(C) TSOI10cm: soil temperature at 10 cm, (D) RAIN: mean annual rainfall, (E) SNOW:

mean annual snowfall, and (F) SOILLIQ10cm: soil water at 10 cm.
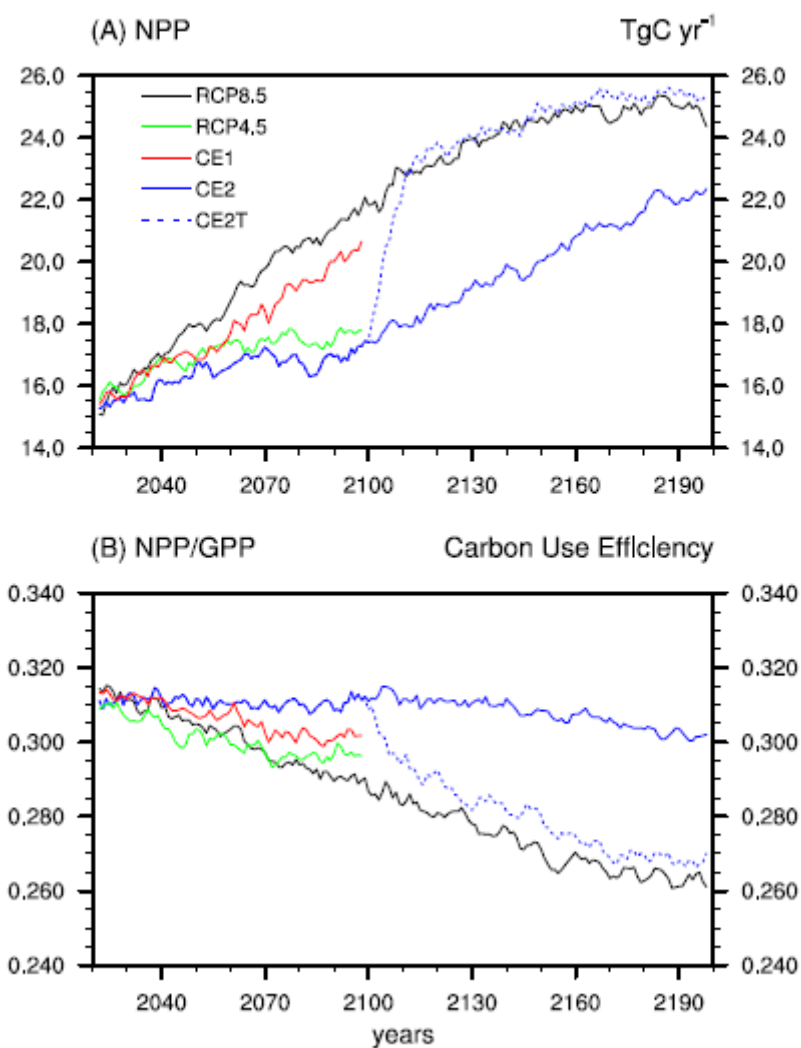
Figure 4

Figure 4. The 5-yr running mean of high latitude NPP (A) and carbon use efficiency (B) for RCP4.5, RCP8.5, CE1, CE2, and CE2T simulations. The values are means of 55-85°N.